Proximity-induced superconducting gap in the quantum spin Hall edge state of monolayer WTe_2

Felix Lüpke,[1,*] Dacen Waters,[1,*] Sergio C. de la Barrera,[1] Michael Widom,[1] David G. Mandrus,[2,3,4] Jiaqiang Yan,[2] Randall M. Feenstra,[1] and Benjamin M. Hunt[1,†]

[1]*Department of Physics, Carnegie Mellon University, Pittsburgh, PA 15213*
[2]*Materials Science and Technology Division, Oak Ridge National Laboratory, Oak Ridge, TN 37831, USA*
[3]*Department of Materials Science and Engineering, University of Tennessee, Knoxville, TN 37996, USA*
[4]*Department of Physics and Astronomy, University of Tennessee, Knoxville, TN 37996, USA*

The quantum spin Hall (QSH) state was recently demonstrated in monolayers of the transition metal dichalcogenide 1T'-WTe_2 and is characterized by a band gap in the two-dimensional (2D) interior and helical one-dimensional (1D) edge states [1–3]. Inducing superconductivity in the helical edge states would result in a 1D topological superconductor, a highly sought-after state of matter [4]. In the present study, we use a novel dry-transfer flip technique to place atomically-thin layers of WTe_2 on a van der Waals superconductor, $NbSe_2$. Using scanning tunneling microscopy and spectroscopy (STM/STS), we demonstrate atomically clean surfaces and interfaces and the presence of a proximity-induced superconducting gap in the WTe_2 for thicknesses from a monolayer up to 7 crystalline layers. At the edge of the WTe_2 monolayer, we show that the superconducting gap coexists with the characteristic spectroscopic signature of the QSH edge state. Taken together, these observations provide conclusive evidence for proximity-induced superconductivity in the QSH edge state in WTe_2, a crucial step towards realizing 1D topological superconductivity in this van der Waals material platform.

A topological superconductor is a state of matter classified by a pairing gap that gives rise to protected gapless excitations at its boundaries. Contemporary interest in topological superconductors has been driven by these gapless excitations, thought to be emergent Majorana quasiparticles with non-abelian statistics [5–8]. One path toward topological superconductivity is to realize an intrinsic spinless p-wave superconductor [9]. A powerful alternative is by using a conventional s-wave superconductor to induce Cooper pairing in topologically non-trivial states via the superconducting proximity effect, resulting in an effective p-wave pairing [10]. This approach has been employed to engineer 2D topological superconductivity in epitaxial topological insulator films grown on a superconducting substrate [11, 12], and 1D topological superconductivity by proximitizing a quantum spin Hall (QSH) state in buried epitaxial semiconductor quantum wells [13, 14]. While such demonstrations mark important milestones, there are clear advantages for exploring topological superconductivity in the van der Waals material platform. Using layered 2D materials allows the 2D QSH edge to be proximitized in vertical heterostructures, circumventing the length restrictions of lateral proximity-effect geometries. Furthermore, the surfaces and edges are readily available for surface probes, allowing detection and fundamental study of signatures of the topological superconducting state.

Following recent theoretical predictions [15], an intrinsic QSH state was demonstrated in a monolayer (ML) of 1T'-WTe_2 [1–3, 16–18]. WTe_2 is attractive for studying the QSH edge modes because it can be readily incorporated in van der Waals heterostructures and has shown quantized edge conductance up to $100\,\mathrm{K}$ [3]. Furthermore, ML WTe_2 was recently also shown to host intrinsic superconducting behavior below $\sim 1\,\mathrm{K}$ when electrostatically gated into the conduction band [19, 20].

In the present work, we study mechanically-exfoliated single- and few-layers of WTe_2 which have been transferred onto a van der Waals s-wave superconductor, $NbSe_2$. We show that this approach induces a superconducting gap in the WTe_2 without the need for electrostatic doping and yields a critical temperature much higher than that of the intrinsic WTe_2 superconductivity, an experimental advantage which greatly facilitates studies of the interplay of superconductivity and the QSH edge modes. We employ scanning tunneling microscopy and spectroscopy (STM/STS) to investigate the proximity-induced superconducting gap as a function of temperature, magnetic field, and WTe_2 thickness. By spatially resolving the spectroscopic features of the WTe_2, we find that the superconducting gap coexists with the QSH signature at the ML WTe_2 edge, demonstrating critical steps toward identifying 1D topological superconductivity in a van der Waals material system.

We have developed a novel fabrication technique which enables the assembly and deterministic placement of van der Waals heterostructures (Fig. 1a). Though similar methods have been used to fabricate complex encapsulated mesoscale devices [21], critically, our technique produces atomically-clean surfaces of air-sensitive materials suitable for scanning probe measurements. Figure 1b shows an STM image of a heterostructure where the WTe_2 ML edge and the underlying $NbSe_2$ are visible, showing atomically-clean surfaces on each material. The height profile across the step edge gives a step height of ~ 7 Å which corresponds to one WTe_2 layer [17], indicating an atomically-clean interface between the WTe_2 and $NbSe_2$. Atomically-resolved STM images of the $NbSe_2$ surface (Fig. 1c) show the well-known 3×3 charge density wave [11], indicating the pristine quality of the $NbSe_2$ substrate. Atomically-resolved STM images of the WTe_2 ML (Fig. 1d) are characterized by vertical atomic rows parallel to the b-axis

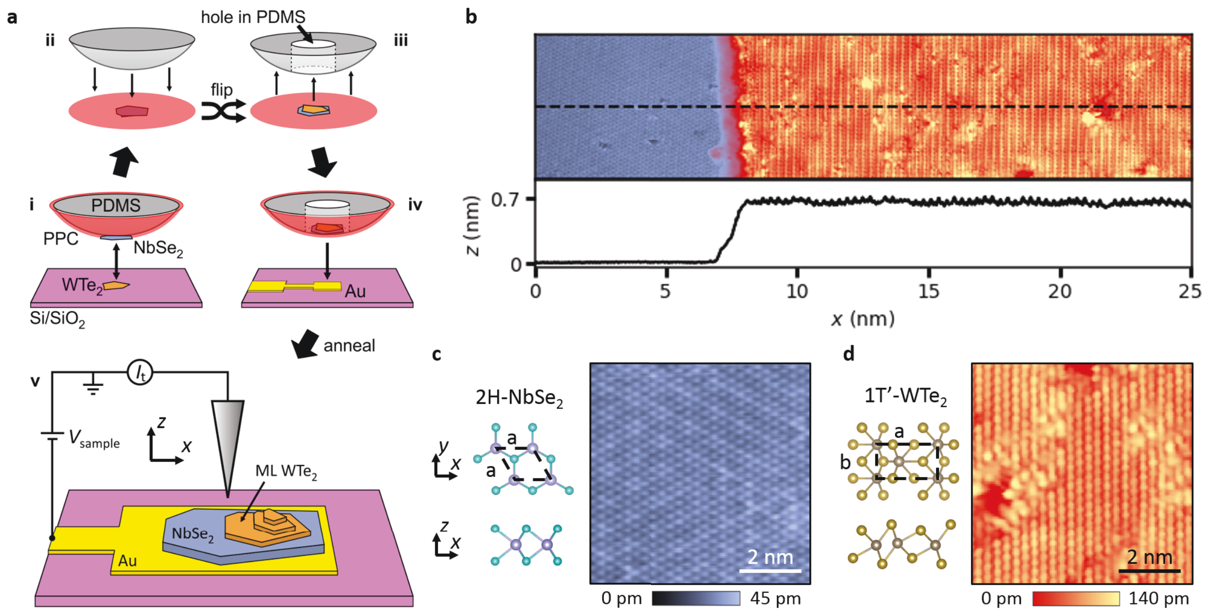

FIG. 1. **Fabrication and morphology of $WTe_2/NbSe_2$ heterostructure. (a)** Schematic of the sample fabrication. After assembly of the $NbSe_2/WTe_2$ heterostructure using a PPC/PDMS stamp (inside a nitrogen-filled glove box), the PPC film is peeled off, flipped upside down and put onto a new PDMS stamp which has a hole in it. This stamp is used to deterministically place the heterostructure onto pre-patterned gold leads without bringing the heterostructure surface into contact with any polymers or solvents. The PPC is then evaporated by annealing under vacuum conditions and the sample is transferred to the STM, all without intermediate air-exposure. **(b)** STM topography and height profile across the edge of the monolayer WTe_2 flake ($V_{\mathrm{sample}} = 300\,\mathrm{mV}$ and $I_{\mathrm{t}} = 10\,\mathrm{pA}$). **(c)** Atomic structures and atomically-resolved STM image of the $NbSe_2$ flake showing the 3×3 CDW ($V_{\mathrm{sample}} = 300\,\mathrm{mV}$ and $I_{\mathrm{t}} = 35\,\mathrm{pA}$). **(d)** Atomic structures and atomically-resolved STM image of ML WTe_2 ($V_{\mathrm{sample}} = 1\,\mathrm{V}$ and $I_{\mathrm{t}} = 55\,\mathrm{pA}$). In (b) a moiré pattern in the form of diagonal stripes can be seen on the ML WTe_2 resulting from the superposition of the two different atomic lattices. While $NbSe_2$ has a hexagonal unit cell with lattice parameters $a = b = 3.44\,\text{Å}$, WTe_2 has a rectangular unit cell with lattice parameters $a = 6.28\,\text{Å}$ and $b = 3.48\,\text{Å}$ (Fig. 1c, d). The moiré pattern, analyzed in more detail in the SI, corresponds to a twist angle of $\approx 3^\circ$. The topographies shown in (b), (c), and (d) are representative of the heterostructure over most of the area of the exfoliated flakes.

of the WTe_2 unit cell. Turning now to spectroscopic analysis of these surfaces, Fig. 2a shows a map of dI/dV spectra taken along a line perpendicular to the WTe_2 monolayer step edge (upper panel) and the corresponding height profile (lower panel). The dI/dV spectra clearly show the presence of an increased local density of states (LDOS) near the WTe_2 step edge. This feature was recently reported in STM/STS studies of ML films of WTe_2 grown on epitaxial graphene substrates [1, 16]. Based on combined evidence from ARPES and STS in Ref. 1, it was concluded that ML WTe_2 has a band gap of $(56 \pm 14)\,\mathrm{meV}$, and that the increased LDOS at the ML WTe_2 edge signifies the metallic QSH edge state. In our monolayer samples, produced via isolation from bulk crystals rather than molecular beam epitaxy, and on superconducting substrates rather than graphene, we observe the same spectroscopic features, which we attribute to the same QSH edge state. Figure 2b shows the averaged dI/dV spectrum on the WTe_2 ML (red) and the ML edge (orange) at the corresponding positions indicated in Fig. 2a. The spectroscopic signature of the QSH edge state is evident primarily in the valence band but, importantly, the edge state also crosses the band gap. Following the interpretation of Ref. 1, the increases in the dI/dV signal at $E - E_{\mathrm{F}} \approx -50\,\mathrm{meV}$ and $E - E_{\mathrm{F}} \approx 15\,\mathrm{meV}$ correspond to the onset of the WTe_2 valence and conduction band, respectively, locating E_F in the ML WTe_2 band gap. A non-zero dI/dV signal in the band gap away from the step edge was proposed to be due to defect states and substrate effects [1]. In addition, tip-induced band bending may play a role in introducing spectral weight in the WTe_2 band gap (see Supplementary Information (SI)). By comparing the positions of the observed spectral features to epitaxially-grown WTe_2 on graphene [1, 16] and exfoliated WTe_2 [22], we conclude that there is no significant charge transfer from the $NbSe_2$ to the WTe_2. This observation is further supported by our density functional theory (DFT) calculations of the ML $WTe_2/NbSe_2$ heterostructure, which show no significant modification of the WTe_2 electronic structure compared to a freestanding ML of WTe_2 (see SI).

Measurements of the ML WTe_2 dI/dV spectrum over a smaller voltage range (Fig. 2c), reveal a new feature: a superconducting gap-like feature centered around the Fermi energy, characterized by a dip in the dI/dV signal with peaks on either side of the gap. Comparison of measurements at $4.7\,\mathrm{K}$ and $2.8\,\mathrm{K}$ show that the gap deepens and the peaks sharpen at lower temperature. The evolution of the superconducting gap-like feature under application of a surface-normal mag-

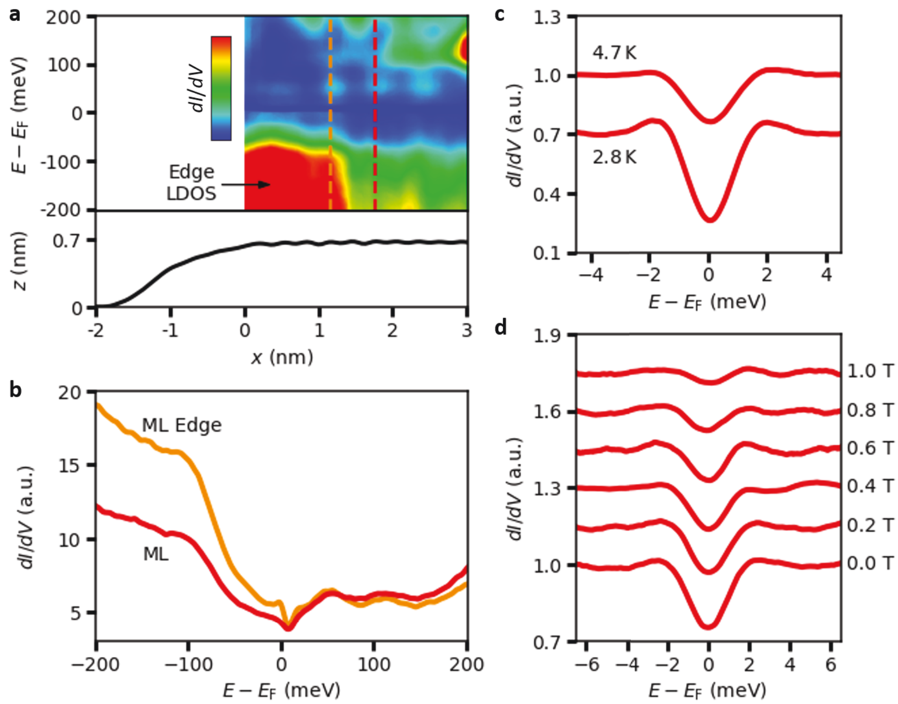

FIG. 2. **Simultaneous presence of quantum spin Hall edge state and superconducting gap in monolayer WTe_2. (a)** dI/dV spectra taken along a line across the step edge of the WTe_2 flake (top), and corresponding height profile (bottom) ($V_{\rm sample} = 300\,\rm mV$ and $I_{\rm t} = 400\,\rm pA$). **(b)** Spatially averaged dI/dV spectra of monolayer WTe_2 showing a representative spectrum away from the monolayer edge (corresponding to the red dashed line in a)) and increased density of states at the monolayer edge due to presence of the QSH edge state (corresponding to orange dashed line in a)). Small voltage range dI/dV spectrum of monolayer WTe_2 at $4.7\,\rm K$ and $2.8\,\rm K$ showing superconducting gap-like features. The $2.8\,\rm K$ curve is offset for clarity. **(d)** Magnetic field dependence of the small voltage spectrum of monolayer WTe_2 measured at $4.7\,\rm K$. The curves are offset for clarity.

netic field at $4.7\,\rm K$ (Fig. 2d) shows that with increasing magnetic field, the gap becomes less deep and the peaks flatten out until the gap features have nearly vanished at $1\,\rm T$. To understand this gap, we fit the observed superconducting-like gap with the Bardeen-Cooper-Schrieffer (BCS) spectrum (see SI). We find that the BCS model fits both the monolayer WTe_2 and the $NbSe_2$ data well (Fig. 3a). For $NbSe_2$, the fit results in a superconducting gap of $\Delta_{\rm NbSe_2} = (0.84 \pm 0.01)\,\rm meV$, while for the WTe_2 it results $\Delta_{\rm WTe_2} = (0.72 \pm 0.02)\,\rm meV$. In addition to following the trend of a superconducting gap with applied magnetic field, the vanishing of the gap near $1\,\rm T$ also agrees with the Ginzburg-Landau estimate for the upper critical field of bulk $NbSe_2$ [23]. We conclude that the gap feature observed on the ML WTe_2 is indeed a superconducting gap.

In order to confirm the proximity-induced nature of the observed superconducting gap, we explore its evolution as a function of WTe_2 thickness. The exfoliation procedure naturally produces terraces of varying thickness in our samples, enabling thickness-dependent gap measurement within a single sample. Figure 3b shows the superconducting gap measured on terraces of different numbers of WTe_2 layers N, revealing that the gap decreases with increasing N, as expected for decaying superconducting correlations near the boundary of a superconducting–metal interface [24]. To quantify this behavior, we fit the BCS model to each of the spectra in Fig. 3b and plot the extracted gap sizes as filled circles in Fig. 3c. In the thick limit ($N\ \geq$3), we find that observed behavior shows excellent agreement with transport measurements of proximity-induced superconductivity in bulk WTe_2 flakes [24, 25], extending the previous studies to the ultra-thin limit (see SI). For $N < 3$, we observe a more rapid decrease of the extracted gap which may be explained by the strong dependence of the electronic structure of the WTe_2 in this thickness range, resulting in a larger mismatch of the WTe_2 and $NbSe_2$ Fermi surfaces and therefore a stronger dependence of the induced gap on N [26].

For monolayer and bilayer WTe_2/$NbSe_2$, we also consider the possibility that the spectra may be a superposition of tunneling into WTe_2 and into $NbSe_2$ (Fig. 4a,b inset). We therefore performed a control experiment, tunneling into ML WTe_2 on a $\sim$$20\,\rm nm$ thick hBN substrate, in order to isolate the relative contributions (Fig. 4a,b). This allows us to perform a more detailed analysis of the ML WTe_2 /$NbSe_2$ spectrum (Fig. 4d) in which we fit a superposition of BCS spectra, with a 14% fractional contribution from ML WTe_2 . The resulting induced gap size is $\Delta^{(ML)}_{\rm WTe_2} = 0.76 \pm 0.16$ meV at 4.7 K and 0.83 ± 0.08 meV at 2.8 K (Fig. 4d). For the bilayer, we find a fractional contribution of 75% and an induced gap

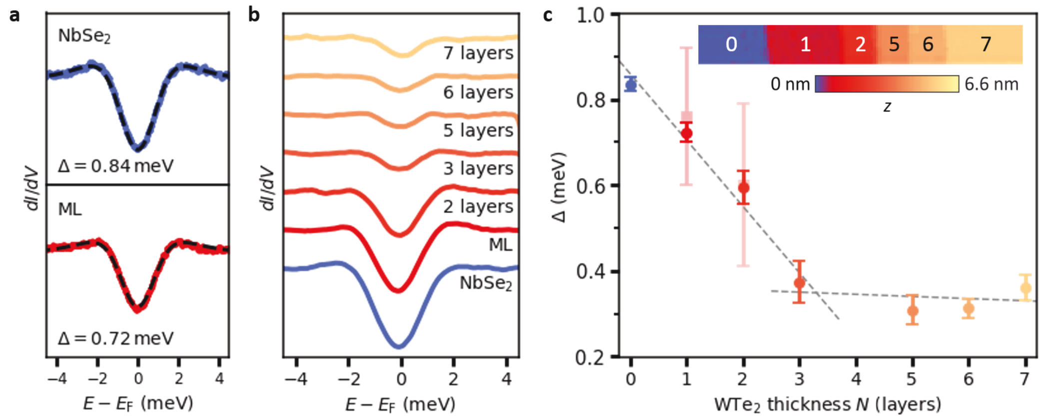

FIG. 3. **Evolution of the superconducting gap with WTe_2 thickness at 4.7 K. (a)** Fits of the BCS model to the superconducting gap spectra measured on $NbSe_2$ and monolayer WTe_2 result in $\Delta_{\mathrm{NbSe_2}} = (0.84 \pm 0.01)$ meV and $\Delta_{\mathrm{WTe_2}} = (0.72 \pm 0.02)$ meV. **(b)** Measurement of the superconducting gap spectrum for WTe_2 layer thicknesses up to 7 layers. **(c)** (filled circles) WTe_2 thickness dependence of the superconducting gap size obtained from fitting the spectra in (b) with the BCS gap equation. (filled squares) Fits of the monolayer and bilayer spectrum with a more detailed model which includes partial tunneling into the $NbSe_2$ substrate. The dashed lines indicate two different regimes in which Δ decreases more rapidly for $N < 3$ and more gradually for $N \geq 3$. The inset shows a large-scale topography image of the WTe_2, where terraces of different WTe_2 thicknesses are observed. Scan size: $200\,\mathrm{nm} \times 14\,\mathrm{nm}$. The corresponding number of WTe_2 layers N is indicated for each terrace, where $N = 0$ is the bare $NbSe_2$.

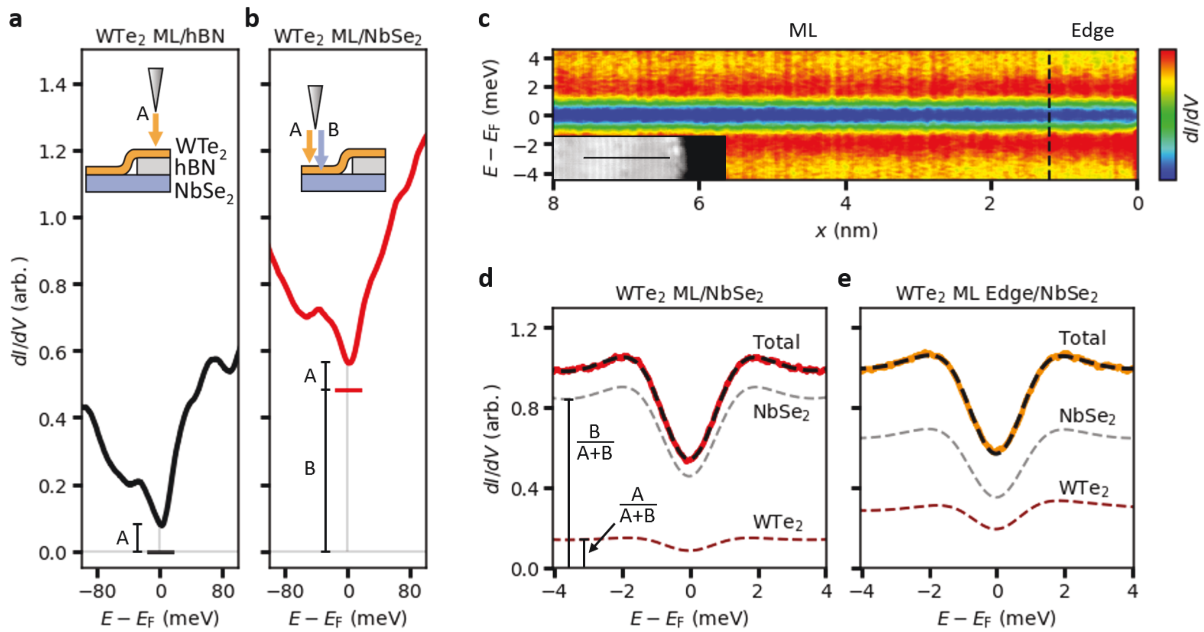

FIG. 4. **Proximity-induced superconducting gap in the quantum spin Hall edge state of monolayer WTe_2 at 2.8 K. (a)** Tunneling spectrum of WTe_2 on hexagonal boron nitride (hBN) and **(b)** spectrum of the *same* WTe_2 flake on $NbSe_2$ (for optical micrograph of the heterostructure see SI). The tunneling contributions of the WTe_2 and $NbSe_2$ are indicated as A and B, respectively. **(c)** SC gap spectra measured along a line perpendicular to the edge of the WTe_2. The inset shows the topography and line along which the spectra were taken. Scan size: $16\,\mathrm{nm} \times 4\,\mathrm{nm}$. **(d)** Fitting of representative ML $WTe_2/NbSe_2$ tunneling spectrum. The fractional contribution of tunneling into WTe_2 is $f_{\mathrm{WTe_2}} \equiv A/(A+B) = 0.14 \pm 0.04$. The $NbSe_2$-derived states contribution is therefore $f_{\mathrm{NbSe_2}} = B/(A+B) = 0.86 \pm 0.04$. The model used to fit the data is $(dI/dV)_{\mathrm{Total}} = f_{\mathrm{WTe_2}} \cdot (dI/dV)_{\mathrm{WTe_2}} + f_{\mathrm{NbSe_2}} \cdot (dI/dV)_{\mathrm{NbSe_2}}$, using a BCS form for each dI/dV (details in SI). The grey and maroon dashed lines indicate the $(dI/dV)_{\mathrm{NbSe_2}}$ and $(dI/dV)_{\mathrm{WTe_2}}$, the proximity-induced SC gap in the WTe_2. The size of the induced gap is $\Delta^{(ML)}_{\mathrm{WTe_2}} = 0.83 \pm 0.08$ meV. **(e)** Fitting of the ML edge $WTe_2/NbSe_2$ tunneling spectrum. We use the same gap(s) found for $NbSe_2$ from (a) and use $\Delta^{(edge)}_{\mathrm{WTe_2}}$ and the new fractional contribution of the WTe_2 edge state, $f^{(edge)}_{\mathrm{WTe_2}}$ as fitting parameters (details in SI). The resulting induced SC gap in the WTe_2 QSH edge state is $\Delta^{(edge)}_{\mathrm{WTe_2}} = 0.75 \pm 0.08$ meV.

of $\Delta^{(BL)}_{\mathrm{WTe_2}} = 0.60 \pm 0.19$ meV. In Fig. 3c we plot the 4.7 K induced gaps and find no significant deviation from those determined by the one-gap fits.

Finally, we consider the lateral variation of the superconducting gap from within the ML WTe_2 to the region occupied by the edge state. Figure 4c shows dI/dV spectra taken at $2.8\,\mathrm{K}$ along a line approaching the physical edge of the WTe_2 monolayer, similar to that shown in Fig. 2a but over a smaller voltage range. The superconducting gap is present throughout the WTe_2 monolayer with only slight changes in the gap width and depth. It is apparent that a superconducting gap is present in the region in which the QSH edge state is observed in Fig. 2a (indicated by the dashed line in Fig. 4c). To confirm that there is a fractional contribution to this spectrum due to an induced gap in the QSH edge state, in Fig. 4e we perform a similar fit as we did for the spectrum $10\,\mathrm{nm}$ away from the edge in Fig. 4d. We find that the induced gap in the edge state has a value of $\Delta^{(edge)}_{\mathrm{WTe_2}} = 0.75 \pm 0.08$ meV. The observation of a gap in the edge state of monolayer 1T'-WTe_2 provides strong evidence that we have created a 1D topological insulator in a van der Waals heterostructure by proximity-induced superconductivity in the quantum spin Hall edge state.

The topological nature of a superconducting QSH edge state could be explicitly demonstrated in an STM measurement by creating a boundary with a portion of the same QSH edge state in which a topologically-trivial gap has been opened [4]. This would localize Majorana zero modes at the boundary, which can be identified as a zero-bias conductance peak within the superconducting gap [27]. Creating such a boundary is straightforward in the van der Waals material platform, e.g., by integrating a van der Waals magnetic insulator into the heterostructure shown in Fig. 1a to open a local Zeeman gap. Our work establishes the groundwork for such an experiment with a clear path toward the realization of Majorana quasiparticles. In addition, the method of sample preparation outlined in this work may be easily adapted to numerous experiments involving surface-probe studies or air-sensitive materials.

METHODS

WTe_2 and $NbSe_2$ were exfoliated onto SiO_2 in a nitrogen-filled glovebox. A WTe_2 flake with regions of different thicknesses was transferred onto a $(20 \pm 1)\,\mathrm{nm}$ thick $NbSe_2$ flake using the technique depicted in Fig. 1a. At this thickness, the electronic properties of the $NbSe_2$ are bulk-like and the critical temperature below which the $NbSe_2$ becomes superconducting is $T_\mathrm{c} \approx 7\,\mathrm{K}$ [28]. For optical images of the sample and further details on the sample fabrication see SI. The STM tip is approached to the WTe_2/$NbSe_2$ heterostructure using a capacitive technique adapted from Ref. [29]. The commercial CreaTec STM helium bath temperature is $4.2\,\mathrm{K}$ with the ability of intermittently reaching $\sim 1\,\mathrm{K}$ by pumping on the cryostat. The resulting STM temperatures are $4.7\,\mathrm{K}$ and $2.8\,\mathrm{K}$, respectively, due to vibration isolation and optical access. The STM is equipped with an electrochemically-etched tungsten tip which was indented into gold prior to and in between measurements. The lock-in frequency was set to $f = 925\,\mathrm{Hz}$ in all dI/dV measurements. All superconducting gap measurements were performed at $V_\mathrm{sample} = 5\,\mathrm{mV}$ with $V_\mathrm{mod} = 100\,\mu\mathrm{V}$ peak-to-peak and $I_\mathrm{t} = 100\,\mathrm{pA}$, except in Fig. 2 e) where $V_\mathrm{sample} = 10\,\mathrm{mV}$. The spectra in Fig. 2 a) and b) were acquired using $V_\mathrm{mod} = 5\,\mathrm{mV}$. In Fig. 4, tunneling parameters are: $V_\mathrm{sample} = 300\,\mathrm{mV}$, $I_\mathrm{t} = 100\,\mathrm{pA}$ and $V_\mathrm{mod} = 5\,\mathrm{mV}$ in (a) and $V_\mathrm{sample} = 300\,\mathrm{mV}$, $I_\mathrm{t} = 110\,\mathrm{pA}$ and $V_\mathrm{mod} = 10\,\mathrm{mV}$ in (b). For quantitative comparison, the two spectra were normalized to the tunneling current and V_mod.

ACKNOWLEDGMENTS

The authors acknowledge Di Xiao, David Cobden and Xiaodong Xu for helpful discussions and Nicholas Speeney and Nicolas Iskos for assistance in the lab. B.M.H. was supported by the Department of Energy under the Early Career award program (#DE-SC0018115). Crystal growth and characterization at ORNL was supported by the US Department of Energy, Office of Science, Basic Energy Sciences, Division of Materials Sciences and Engineering. The authors thank the Pennsylvania State University Two-Dimensional Crystal Consortium - Materials Innovation Platform (2DCC-MIP) which is supported by NSF DMR-1539916 for supplying further 2D materials. F.L. and D.W. were supported by the NSF DMR-1809145) for the STM measurements. The authors gratefully acknowledge NSF DMR-1626099 for acquisition of the STM instrument. S.C.d.l.B. was supported by the Department of Energy (#DE-SC0018115) for fabrication of proximity-effect van der Waals heterostructures. DFT Calculations were supported by the DOE under grant #DE-SC0014506.

AUTHOR CONTRIBUTIONS

F.L., D.W., R.M.F. and B.M.H. designed the experiment. F.L. and D.W. acquired the experimental data and F.L., D.W., and R.M.F. analyzed the data and performed the fitting to the spectra. F.L., D.W. and S.C.d.l.B. fabricated the samples. F.L., D.W., S.C.d.l.B. and B.M.H. wrote the manuscript, and all authors commented on the manuscript. J.Y. grew the WTe_2 crystals. D.M. provided other van der Waals crystals used in this study. M.W. performed DFT calculations. R.M.F. and B.M.H. supervised the project.

* These authors contributed equally.
† bmhunt@andrew.cmu.edu

[1] Tang, S. *et al.* Quantum spin Hall state in monolayer $1T' - \mathrm{WTe_2}$. *Nat. Phys.* **13**, 683 (2017).

[2] Fei, Z. *et al.* Edge conduction in monolayer $\mathrm{WTe_2}$. *Nat. Phys.* **13**, 677 (2017).

[3] Wu, S. *et al.* Observation of the quantum spin Hall effect up to 100 Kelvin in a monolayer crystal. *Science* **359**, 76–79 (2018).

[4] Alicea, J. New directions in the pursuit of Majorana fermions in solid state systems. *Rep. Prog. Phys.* **75**, 076501 (2012).

[5] Kitaev, A. Y. Unpaired Majorana fermions in quantum wires. *Phys.-Uspekhi* **44**, 131–136 (2001).

[6] Fu, L. & Kane, C. L. Superconducting proximity effect and Majorana fermions at the surface of a topological insulator. *Phys. Rev. Lett.* **100**, 096407 (2008).

[7] Sarma, S. D., Freedman, M. & Nayak, C. Majorana zero modes and topological quantum computation. *npj Quantum Inf.* **1**, 15001 (2015).

[8] Sato, M. & Ando, Y. Topological superconductors: a review. *Rep. Prog. Phys.* **80**, 076501 (2017).

[9] Maeno, Y., Kittaka, S., Nomura, T., Yonezawa, S. & Ishida, K. Evaluation of spin-triplet superconductivity in Sr_2RuO_4. *J. Phys. Soc. Jpn.* **81**, 011009 (2012).

[10] Fu, L. & Kane, C. L. Josephson current and noise at a superconductor/quantum-spin-Hall-insulator/superconductor junction. *Phys. Rev. B* **79**, 161408 (2009).

[11] Wang, M.-X. *et al.* The coexistence of superconductivity and topological order in the Bi_2Se_3 thin films. *Science* **336**, 52–55 (2012).

[12] Sun, H.-H. *et al.* Majorana zero mode detected with spin selective Andreev reflection in the vortex of a topological superconductor. *Phys. Rev. Lett.* **116**, 257003 (2016).

[13] Hart, S. *et al.* Induced superconductivity in the quantum spin Hall edge. *Nat. Phys.* **10**, 638–643 (2014).

[14] Bocquillon, E. *et al.* Gapless Andreev bound states in the quantum spin Hall insulator HgTe. *Nat. Nanotechnol.* **12**, 137 (2016).

[15] Qian, X., Liu, J., Fu, L. & Li, J. Quantum spin Hall effect in two-dimensional transition metal dichalcogenides. *Science* **346**, 1344–1347 (2014).

[16] Jia, Z.-Y. *et al.* Direct visualization of a two-dimensional topological insulator in the single-layer $1T^{'} - \mathrm{WTe_2}$. *Phys. Rev. B* **96**, 041108 (2017).

[17] Peng, L. *et al.* Observation of topological states residing at step edges of $\mathrm{WTe_2}$. *Nat. Commun.* **8**, 659 (2017).

[18] Shi, Y. *et al.* Imaging quantum spin Hall edges in monolayer $\mathrm{WTe_2}$. *Sci. Adv.* **5** (2019).

[19] Fatemi, V. *et al.* Electrically tunable low-density superconductivity in a monolayer topological insulator. *Science* **362**, 926 (2018).

[20] Sajadi, E. *et al.* Gate-induced superconductivity in a monolayer topological insulator. *Science* **362**, 922 (2018).

[21] Zeng, Y. *et al.* High-quality magnetotransport in graphene using the edge-free Corbino geometry. *Phys. Rev. Lett.* **122**, 137701 (2019).

[22] Cucchi, I. *et al.* Microfocus laserangle-resolved photoemission on encapsulated mono-, bi-, and few-layer $1T^{'} - \mathrm{WTe_2}$. *Nano Lett.* **19**, 554–560 (2019).

[23] Garoche, P., Veyssi, J. J., Manuel, P. & Molini, P. Experimental investigation of superconductivity in 2H-$NbSe_2$ single crystal. *Solid State Commun.* **19**, 455–460 (1976).

[24] Huang, C. *et al.* Inducing strong superconductivity in $\mathrm{WTe_2}$ by a proximity effect. *ACS Nano* **12**, 7185–7196 (2018).

[25] Li, Q. *et al.* Proximity-induced superconductivity with subgap anomaly in type II Weyl semi-metal $\mathrm{WTe_2}$. *Nano Lett.* **18**, 7962–7968 (2018).

[26] Reeg, C. R. & Maslov, D. L. Hard gap in a normal layer coupled to a superconductor. *Phys. Rev. B* **94**, 020501 (2016).

[27] Nadj-Perge, S. *et al.* Observation of Majorana fermions in ferromagnetic atomic chains on a superconductor. *Science* **346**, 602–607 (2014).

[28] Khestanova, E. *et al.* Unusual suppression of the superconducting energy gap and critical temperature in atomically thin $NbSe_2$. *Nano Lett.* **18**, 2623–2629 (2018).

[29] Li, G., Luican, A. & Andrei, E. Y. Self-navigation of a scanning tunneling microscope tip toward a micron-sized graphene sample. *Rev. Sci. Instrum.* **82**, 073701 (2011).